Since January 2020 Elsevier has created a COVID-19 resource centre with free information in English and Mandarin on the novel coronavirus COVID-19. The COVID-19 resource centre is hosted on Elsevier Connect, the company's public news and information website.

Elsevier hereby grants permission to make all its COVID-19-related research that is available on the COVID-19 resource centre - including this research content - immediately available in PubMed Central and other publicly funded repositories, such as the WHO COVID database with rights for unrestricted research re-use and analyses in any form or by any means with acknowledgement of the original source. These permissions are granted for free by Elsevier for as long as the COVID-19 resource centre remains active.

Bioorganic & Medicinal Chemistry Letters 29 (2019) 126717

Contents lists available at ScienceDirect

Bioorganic & Medicinal Chemistry Letters

journal homepage: www.elsevier.com/locate/bmcl

Discovery of novel Cyclophilin D inhibitors starting from three dimensional fragments with millimolar potencies

Ulrich Grädler[a,*], Daniel Schwarz[a], Michael Blaesse[d], Birgitta Leuthner[a], Theresa L. Johnson[a], Frederic Bernard[b], Xuliang Jiang[b], Andreas Marx[a], Marine Gilardone[c], Hugues Lemoine[c], Didier Roche[c], Catherine Jorand-Lebrun[b]

[a] *Merck Healthcare, Merck KGaA, Frankfurter Str. 250, D-64293 Darmstadt, Germany*
[b] *EMD Serono Research & Development Institute Inc., 45A Middlesex Turnpike, Billerica, MA 01821, USA*
[c] *Edelris, 115 Avenue, Lacassagne, F-69003 Lyon, France*
[d] *Proteros Biostructures GmbH, Bunsenstraße 7a, D-82152 Planegg-Martinsried, Germany*

ARTICLE INFO

Keywords:
Cyclophilin D
Inhibitor
Fragment-screening
X-ray structure
Surface plasmon resonance
Structure-based design
Fragment-based lead discovery

ABSTRACT

Fragment-based screening by SPR enabled the discovery of chemical diverse fragment hits with millimolar binding affinities to the peptidyl-prolyl isomerase Cyclophilin D (CypD). The CypD protein crystal structures of 6 fragment hits provided the basis for subsequent medicinal chemistry optimization by fragment merging and linking yielding three different chemical series with either urea, oxalyl or amide linkers connecting millimolar fragments in the S1′ and S2 pockets. We successfully improved the in vitro CypD potencies in the biochemical FP and PPIase assays and in the biophysical SPR binding assay from millimolar towards the low micromolar and submicromolar range by > 1000-fold for some fragment derivatives. The initial SAR together with the protein crystal structures of our novel CypD inhibitors provide a suitable basis for further hit-to-lead optimization.

Cyclophilins are peptidyl-prolyl isomerases (PPIase) catalyzing the *cis–trans* interconversion of proline peptide bonds during protein folding.[1,2] The human cyclophilin protein family consists of 17 highly conserved isoforms, which are abundantly and ubiquitously present in a wide range of tissue types and organisms with functions beyond protein maturation.[2,3] Among them, Cyclophilin A (CypA) is the major cellular target of the immunosuppressive drug cyclosporin A (CsA, Fig. 1) forming a ternary complex with calcineurin and thus preventing regulation of cytokine gene transcription.[4–6] Cyclophilins also play a key role in pathophysiological processes such as inflammation and vascular dysfunction, wound healing, innate HIV immunity, hepatitis C infection, host-parasite interactions and tumor biology.[7] Cyclophilin D (CypD) is the mitochondrial isoform of the enzyme, and a key regulator of the mitochondrial permeability transition pore. Mitochondrial dysfunction has been implicated in a cascade of cellular processes linked to multiple sclerosis and cardiovascular disease, making CypD a therapeutic drug target.[7–10] The crystal structures of several cyclophilins have been determined and show a common fold consisting of two α-helices packing against an eight-stranded anti-parallel P-barrel structure.[11] The cyclophilins contain a large active binding groove composed by several highly conserved hydrophobic, aromatic and polar residues including the catalytic Arg55 located at the entrance of the S1′ proline pocket.[2,12] A second S2 pocket has been identified nearby: it is deep and relatively non-specific, with access controlled by a set of gatekeeper residues.[2] The cyclic peptide CsA binds via specific interactions involving both S1′ and S2 pockets with nanomolar potency to cyclophilins, e.g. to CypD with a PPIase IC_{50} of 20 nM.[13] However, CsA and its semisynthetic analogues such as Debio 025 and NIM811 have unfavorable drug-like properties due to high molecular weight, limited solubility and poor bioavailability.[14,15] Only few small and non-peptidic CypD inhibitors have been published including urea derivatives such as **2**, which were discovered by fragment-based lead discovery (Fig. 1).[10,16,17] These urea derivatives demonstrated in vitro PPIase inhibitory activity and antiviral activity against hepatitis C virus, human immunodeficiency virus and coronaviruses.[16] Protein crystallography of **2** in CypD revealed specific binding of the pyrrolidine ring in the S1′ pocket, while the aniline substituent is bound in the S2 pocket (Supporting information).[13] Our aim was to identify novel chemical hit matter from HTS and fragment screening approaches to develop CypD inhibitors with drug-like properties for prevention of mitochondrial dysfunction in multiple sclerosis.

We started our hit identification efforts by high-throughput

---

* Corresponding author.
E-mail address: ulrich.graedler@merckgroup.com (U. Grädler).

https://doi.org/10.1016/j.bmcl.2019.126717
Received 13 August 2019; Received in revised form 19 September 2019; Accepted 21 September 2019
Available online 16 October 2019
0960-894X/ © 2019 Elsevier Ltd. All rights reserved.

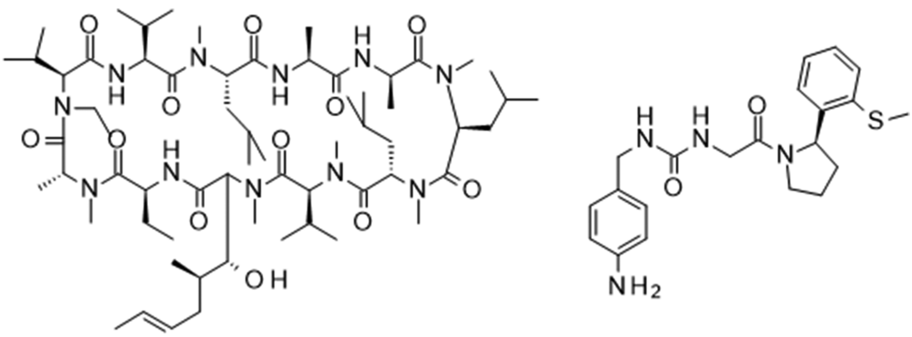

1, Cyclosporine A
SPR: K_D = 30 nM
PPlase assay: IC_{50} = 20 nM

2, University Montpellier
SPR: K_D = 230 nM
PPlase assay: IC_{50} = 600 nM

Fig. 1. Published CypD inhibitors (**1–2**).

screening on our corporate compound library with ~650,000 compounds using an FP biochemical assay, which resulted in only a small hit rate of 178 hits with IC_{50}s < 10 µM. Disappointingly, none of these hits could be confirmed in orthogonal biophysical CypD binding assays using surface plasmon resonance (SPR) and protein-based NMR studies. Due to this outcome, we conducted an additional fragment-based screening campaign using our internal fragment library with 2688 structurally diverse fragments (Supporting information). The fragments were screened by SPR at fixed concentrations of 2 mM using immobilized CypD protein and yielded 168 primary hits. For subsequent hit confirmation, we used CsA at 200 nM for SPR-based competition experiments in compound titration series of 10 concentrations up to 10 mM. The affinity determination by SPR confirmed 58 hits with steady state dissociation constants ($K_{D,ss}$) in the range of 1 mM to > 10 mM. The identified fragments represented a large chemical diversity consisting of different aromatic as well as saturated rings as potential proline-mimicking motifs. However, the fragments had only millimolar potencies and overall low ligand efficiencies (LEs 0.1–0.3 kcal/heavy atom) beyond the high LE range of > 0.3 kcal/heavy atom considered as optimal starting point for fragment optimization.[18,19] We therefore aimed to determine the binding mode in the CypD binding groove for as many fragments as possible by protein crystallography for structure-guided optimization. We evaluated 52 fragments by co-crystallization and by soaking into apo crystals of the CypD K175I mutant and obtained 6 crystal structures with clearly defined fragment electron densities in the active site at resolutions of 1.15–2.0 Å (Table 1 and Supporting information).[20] The 6 fragments displayed a certain variety of binding modes within the CypD binding groove: **3** and **4** are bound in the gatekeeper S2 pocket, **5–7** are located in the proline S1′ pocket and **8** is targeting both S1′ and S2 pockets (Supporting information). All fragment X-ray structures were superimposed with published CypD structures in complex with CsA and urea derivatives such as **2** to define promising fragment linking and merging strategies for hit optimization. These considerations provided the basis of three hit series followed up by medicinal chemistry to improve potency in the biochemical FP and SPR binding assays.

The superimposition of CypD crystal structures in complex with the three-dimensional fragment **3** (K_D = 7.1 mM, LE = 0.2) and the published urea derivative **2** (PDB-ID: 4J5B) indicated almost perfect matching of the aniline rings in the S2 pocket. The annulated tetrahydropyran ring of **3** binds in a lipophilic sub pocket, which becomes accessible by side chain movement of Arg124 (Fig. 2). Furthermore, the fluorine atom of **3** provided a suitable exit vector towards the urea for fragment merging. We prepared a series of urea derivatives by incorporating the bicyclic fragment **3** in combination with the pocket S1′ substituent of **2** as different stereoisomers according to Scheme 1.[21]

Table 1
Overview of SPR-confirmed hits from fragment screening against human CypD confirmed by X-ray crystallography.

Compound	Structure	CypD		Binding mode[c]	Crystal structure PDB ID
		K_D (mM)[a]	LE[b]		
3	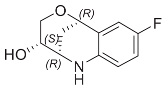	7.1	0.2	S2 pocket	6R9S
4	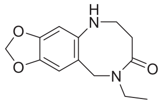	7.5	0.16	S2 pocket	6R9U
5	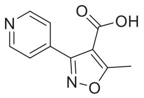	> 10		S1′ pocket	
6	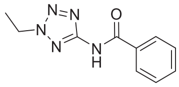	3.9	0.21	S1′ pocket	
7	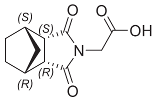	> 10		S1′ pocket	6RA1
8	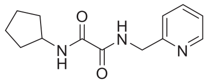	1.1	0.22	S1′ & S2 pocket	6R9X

[a] CypD SPR binding assay.
[b] Ligand binding efficiencies (LE) based on the SPR K_Ds.
[c] Fragment binding location in the CypD pocket from protein crystallization.

The resulting urea derivatives **14–19** showed a clear SAR in the biochemical FP assay as well as in the CypD SPR assay regarding stereochemistry (Table 2). The most potent derivative **14** (FP IC_{50} = 60 nM, PPIase IC_{50} = 4 nM, SPR K_D = 6 nM) had the same stereochemistry as the bicyclic fragment **3** (2*R*,3*S*,6*R*-enantiomer) and the *S*-methylphenyl substituent of **2** (*R*-enantiomer), which corresponds to their binding modes in the crystal structure. Fragment merging towards urea **14** resulted in significant potency improvements compared to the starting urea **2** (FP IC_{50} = 750 nM, SPR K_D = 230 nM) of 12- or 40-fold referring to the FP and SPR assays respectively. The corresponding derivative **15** with the S-methylphenyl substituent as *S*-enantiomer was significantly less potent (FP IC_{50} = 3.6 µM, SPR K_D = 630 nM). Also, the combination of the bicyclic fragment **3** as different stereo isomer (2*S*,3*S*,6*S*-enantiomer) and the *S*-methylphenyl substituent of **2** as *R*-enantiomer resulted in a clear potency drop (**16**: FP IC_{50} = 1.7 µM, SPR

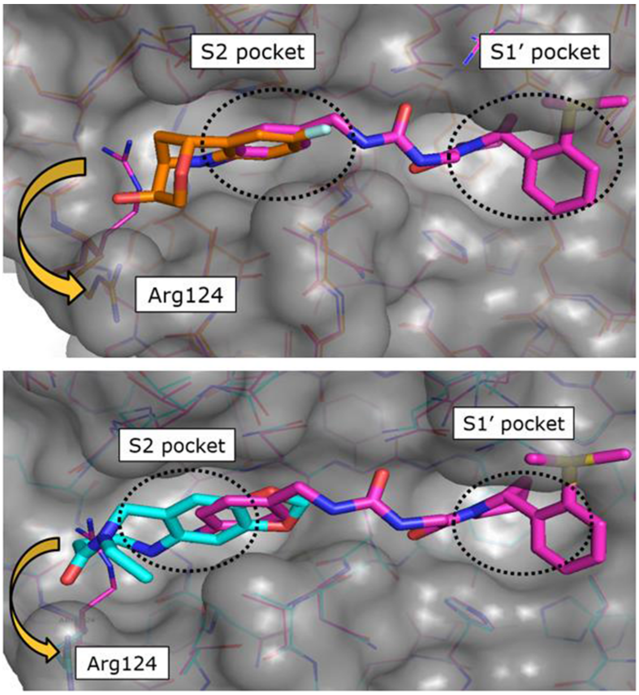

Fig. 2. Superimpositions of CypD crystal structures in complex with published CypD inhibitor **2** (magenta, PDB-ID: 4J5B) and fragment hits **3** (orange, PDB-ID: 6R9S) and **4** (cyan, PDB-ID: 6R9U) indicated identical binding positions of the aniline rings in the S2 pocket. The annulated rings of **3** and **4** bind in a lipophilic sub pocket, which becomes accessible by side chain movement of Arg124.

K_D = 670 nM). For further analysis, we solved the CypD X-ray structures in complex with **14** (PDB-ID: 6R8O) and **16** (PDB-ID: 6R8L) at 1.4 Å and 1.6 Å resolution respectively (Fig. 3). Superimposition of both structures showed complete overlap of the urea groups including direct and water-mediated H-bonds to Arg97 and His96 as well as of the pocket S1′ substituents. The bicyclic rings of **14** and **16** also overlap regarding the NH-groups, which form H-bonds to the backbone carbonyl O-atom of Thr149 on one side and to 'water molecule 1' on the other side. In the crystal structure with **14**, the 'water molecule 1' forms five H-bonds to the backbone atoms of Ser152, Gln153, Gln116 as well as to the OH group of the bicyclic ring, which has also H-bonds to Ser123 and Ser152. In contrast, the position of the **16** OH-group is completely shifted and not in H-bond contact to 'water molecule 1', which is involved in a more ideal tetrahedral H-bond network. In the structure with **16**, the OH-group forms two H-bonds to Ser123 and to 'water molecule 2'.

This altered H-bond network and water co-ordination might contribute to the potency differences observed for **14** (SPR K_D = 6 nM) and **16** (SPR K_D = 670 nM). The potency contribution of the 3-OH-tetrahydropyrane part of the bicyclic ring is demonstrated by the tetrahydroquinoline derivate **17**, which is significantly less active (FP IC_{50} = 3.5 μM, PPIase IC_{50} = 7.4 μM). Modifications of the urea linker either by *N*-methyl substitution (**18**: FP IC_{50} = 1.7 μM) or by amide replacement (**19**: FP IC_{50} = 54 μM) also resulted in large potency drops.

We also evaluated the second three-dimensional fragment **4** (K_D = 7.5 mM, LE = 0.16) for similar merging with the urea derivative **2** by analyzing the superimposed crystal structures (Fig. 2). In this case, the 8-membered lactam ring of **4** is again located in a lipophilic sub cavity formed by induced fit of Arg124 within the S2 pocket. However, the aniline rings have significantly shifted positions (*N*-atom distance ~1.8 Å) resulting in suboptimal exit vectors for fragment merging with the urea group. Consequently, we prepared derivatives **20**–**23** with urea and amide linkers of different length merging the lactam ring of **4** with **2** as *R*-enantiomer (Table 2). The most potent analogue was the methylene urea derivative **20** (FP IC_{50} = 190 nM, SPR K_D = 180 nM), while the urea directly attached to the aromatic ring of **4** resulted in complete loss of binding affinity (**21**: FP IC_{50} > 10 μM). The amide derivatives **22** and **23** with different chain lengths were also less potent (**22**: FP IC_{50} = 4.1 μM, **23**: FP IC_{50} > 10 μM).

Fragment hit **8** (K_D = 1.1 mM, LE = 0.22) binds with its cyclopentyl and 2-pyridine substituents in the S1′ and S2 pockets respectively, which are linked by an oxalyl group in H-bond contact to the Asn144 backbone atoms and the His168 side chain on one side (Supporting information). The side chain of Gln105 is not oriented in optimal angle towards the oxalyl carbonyl and NH-groups on the other side, but forms H-donor π-interactions as calculated with the software tool View-Contacts.[22] The oxalyl group of fragment hit **8** overlaps with the urea of **2** and provides therefore an alternative strategy for linking the three-dimensional fragments **3** and **4** with S2 pocket substituents (Supporting information). The crystal structure superimposition of fragment hits **3** and **8** indicated a certain positional shift of the aniline and pyridine rings. We therefore prepared a series of oxalyl derivatives **27**–**32** from merging the bicyclic ring of fragment **3** with the cyclopentyloxalyl core of **8** with methylene and ethylene linkers according to Scheme 2.[23]

The most potent analogue **27** achieved a > 1000-fold potency enhancement in the biochemical assays (FP IC_{50} = 2 μM, PPIase IC_{50} = 1.5 μM) as well as in the SPR assay (K_D = 2.8 μM) compared to the millimolar potencies of the individual fragments **3** and **8** (Table 3).

Derivative **27** contains the bicyclic fragment **3** in the preferred stereochemistry (2*R*,3*S*,6*R*-enantiomer) as observed for **14** and an ethylene linker attached to the oxalyl group. The alternative analogues **28**–**32** with different bicyclic stereochemistry and/or methylene linkers are less potent or inactive (**28**: FP IC_{50} = 44 μM, **29**–**30**: FP IC_{50} > 100 μM). We also evaluated a similar merging strategy of the

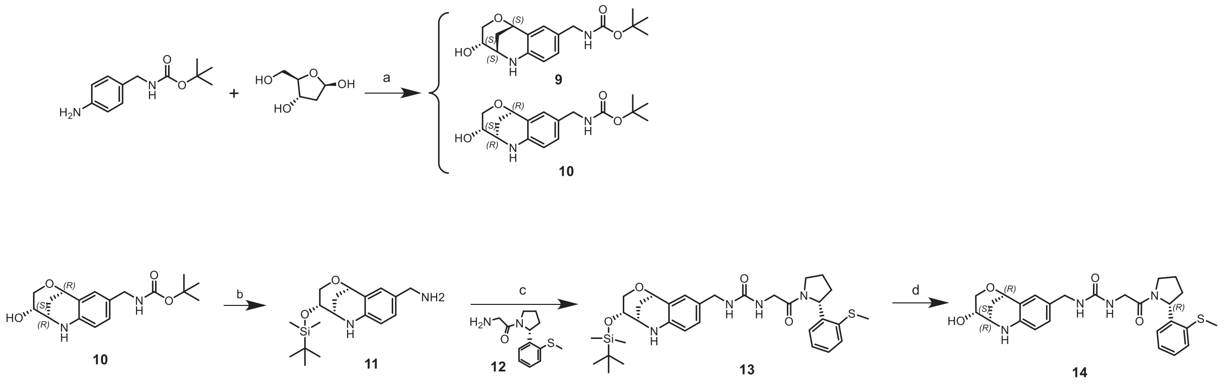

Scheme 1. Reagents and conditions: (a) Montmorillonite in MeCN at RT for 5 d; (b) step 1: lutidine, TBDMSOTf in DCM at 0 °C → RT for 4 h, step 2: TFA in DCM at 0 °C → RT for 1 h; (c) CDI in DCM at RT for 1 h, **12** in THF at 60 °C for 16 h; (d) HF.Pyr in THF at RT for 5 h.

Table 2
CypD SAR of optimized ureas derived from merging of fragments **3** or **4** with the reference inhibitor **2**.

#	Structure	Biochemical CypD FP assay		Biochemical PPIase assay IC_{50} (μM)[c]	SPR binding CypD	
		IC_{50} (μM)[a]	LE[b]		K_D (μM)[d]	LE[e]
14	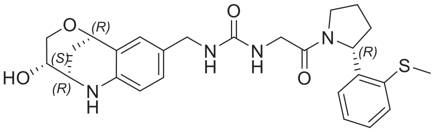	0.060	0.28	0.004	0.006	0.31
15	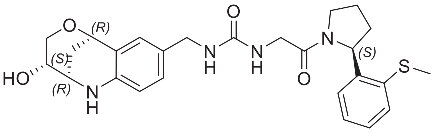	3.6	0.21	nt	0.630	0.23
16	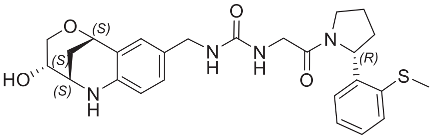	1.7	0.23	nt	0.670	0.23
17	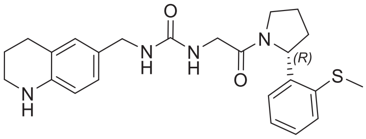	3.5	0.24	7.4	1.10	0.25
18	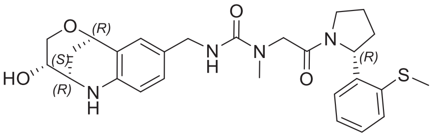	10	0.19	nt	7.0	0.19
19	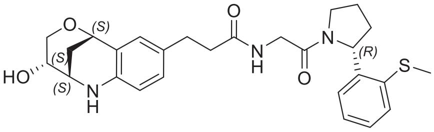	54	0.17	nt	39	0.17
20	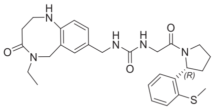	0.190	0.26	nt	0.180	0.25
21	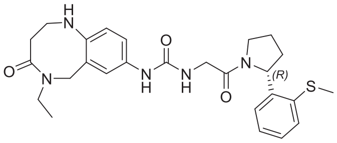	> 100		nt	260	0.13
22	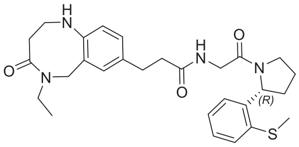	4.1	0.21	nt	2.3	0.21
23	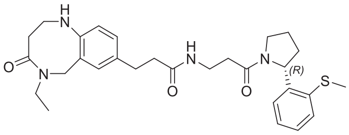	> 100		nt	420	0.12

[a,b]CypD biochemical FP and PPIase assays. [c,e]Ligand binding efficiencies (LE) based on biochemical FP IC_{50}s or SPR K_Ds. [d]CypD SPR binding assay. nt = not tested.

lactam fragment **4** in combination with **8**, but the analogues were again less potent (data not shown). Finally, we replaced the cyclopentyl ring of **27** by the *S*-methylphenyl substituent of **2** as *R*-enantiomer to gain additional potency by more optimized interactions in the S1′ pocket. But the resulting analogues did not show improved potencies (**31**: FP IC_{50} > 100 μM, **32**: FP IC_{50} > 30 μM).

The protein crystal structure determination of the bicyclic fragment hit **7** (K_D > 10 mM) failed by soaking into apo-crystals and by co-crystallization, but we succeeded to solve the structure by soaking of **7** into CypD co-crystals with **4**. In the crystal structure, the fragment **7** binds as (1*S*,2*R*,6*S*,7*R*)-enantiomer in the S1′ proline pocket and forms H-bonds via one of the maleimide carbonyl O-atoms to Ala143 and His168 (Supporting information). The carboxylic acid of **7** is in ionic and H-bond contact to Arg97 and Gln105 respectively and points towards the S2 pocket. The shortest distance between one of the carboxylic O-atoms of **7** and the 1,3-benzodioxole C-atom of the co-crystallized fragment **4** is 3.3 Å, which promptly suggested fragment linking by 1–2 atom linkers (Fig. 4). We considered a more chemically stable amide instead of an ester for linking the bicyclic fragment **7** and the lactam fragment **4** and prepared a series of amides according to Scheme

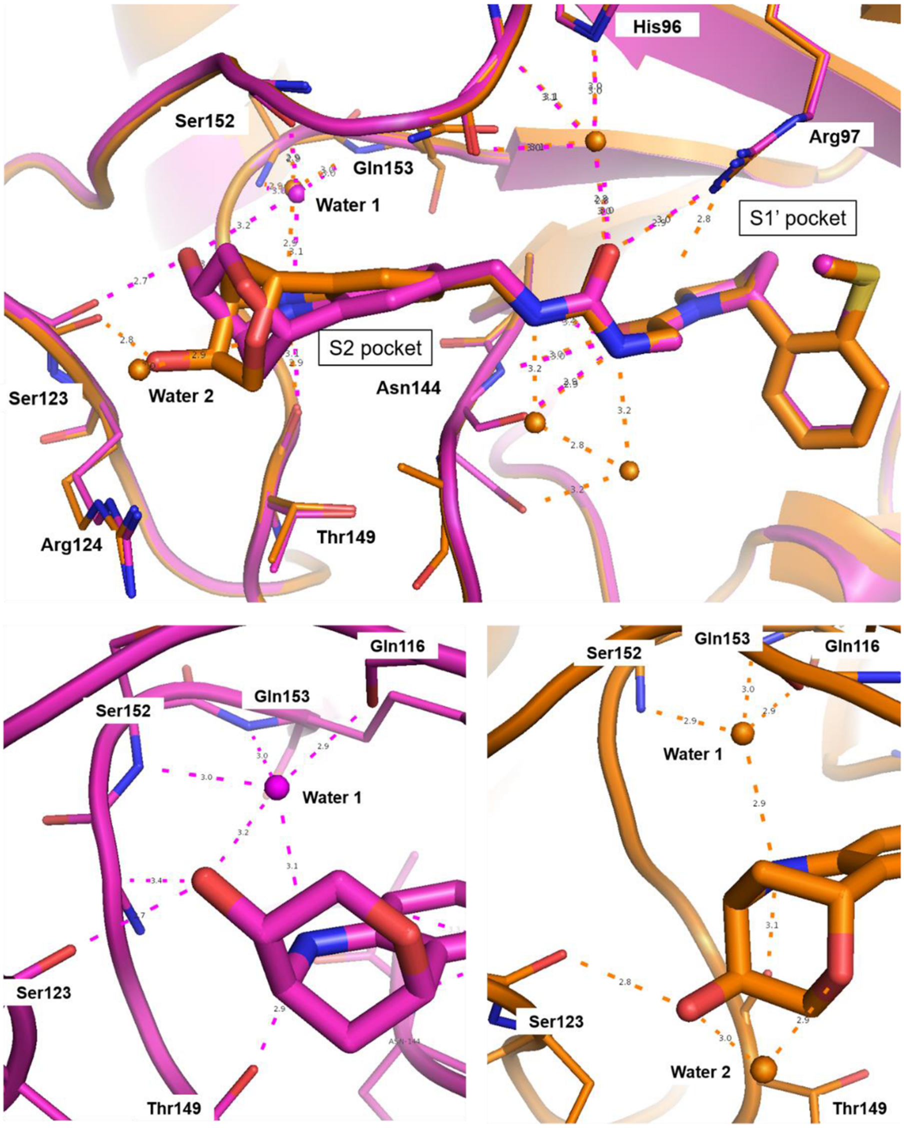
His96
Ser152
Gln153
Arg97
Water 1
S1' pocket
S2 pocket
Water 2
Ser123
Asn144
Arg124
Thr149
Gln116
Ser152
Gln153
Water 1
Ser123
Thr149
Gln153
Ser152
Gln116
Water 1
Ser123
Water 2
Thr149

Fig. 3. Overlay of CypD X-ray structures in complex with **14** (orange, PDB-ID: 6R8O) and **16** (magenta, PDB-ID: 6R8L) at 1.4 Å and 1.6 Å resolution respectively. H-bonds are displayed as dashed lines (hydrogen atoms are omitted and only water molecules in H-bond contact to the inhibitors are shown for clarity). The different stereochemistry of the bicyclic rings results in altered H-bond networks involving the OH-groups and water molecules 1 and 2.

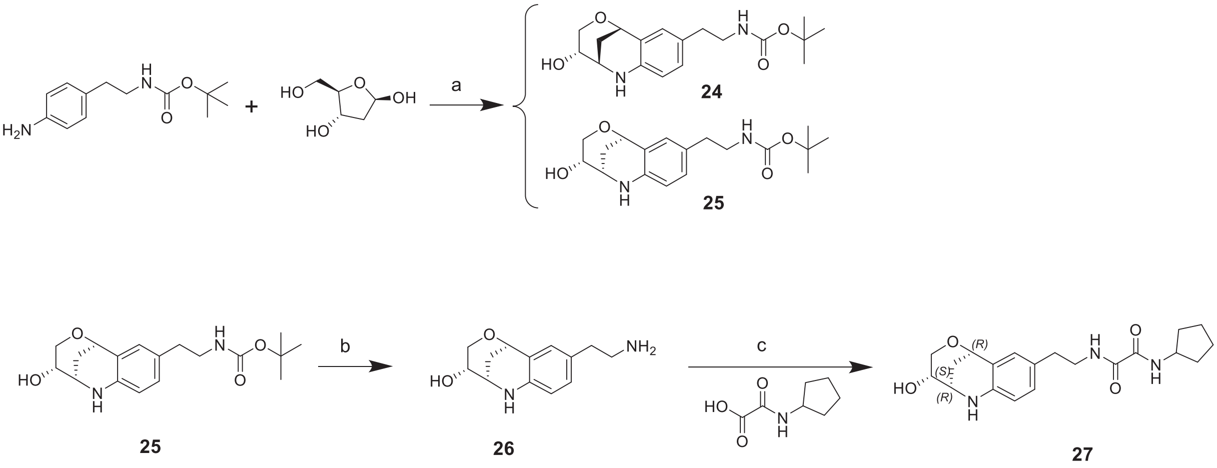
a
24
25
b
c
25
26
27
(R)
(S)
(R)

Scheme 2. Reagents and conditions: (a) Montmorillonite in MeCN at RT for 3 d; (b) TFA in DCM at 0 °C → RT for 1 h; (c) EDCI, HOPO and DIPEA in DMF at RT for 24 h.

Table 3
CypD SAR of optimized oxalamides derived from merging the fragment hits **3** or **4** with fragment hit **8**.

#	Structure	Biochemical CypD FP assay		Biochemical PPIase assay IC_{50} (μM)[c]	SPR binding CypD	
		IC_{50} (μM)[a]	LE[b]		K_D (μM)[d]	LE[e]
27	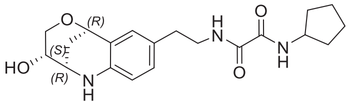	2	0.29	1.5	2.8	0.28
28	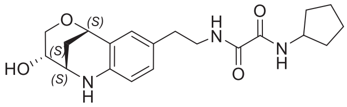	44	0.22	nt	23	0.21
29	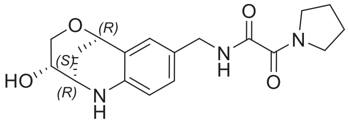	> 100		nt	> 1500	
30	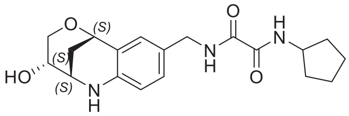	870	0.16	nt	217	0.19
31	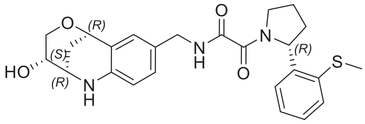	> 100		nt	184	0.16
32	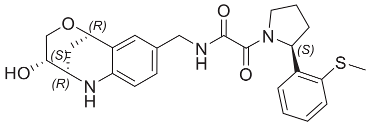	> 30		nt	> 240	

[a,b]CypD biochemical FP and PPIase assays. [c,e]Ligand binding efficiencies (LE) based on biochemical FP IC_{50}s or SPR K_Ds. [d]CypD SPR binding assay. nt = not tested.

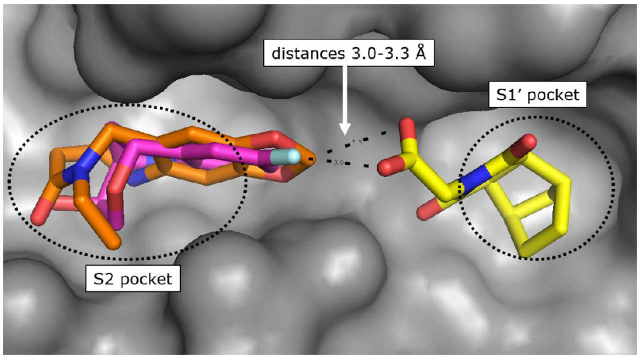

Fig. 4. CypD X-ray structure in ternary complex with fragment hits **7** (yellow) and **4** (orange, PDB-ID: 6R9U) superimposed with X-ray structure in complex with fragment hit **3** (magenta, PDB-ID: 6R9S).

3.[24]

The benzolactam analogue **34** linked by a *N*-methylamide group to the bicyclic ring of fragment **7** showed a modest potency improvement (Table 4, **34**: FP $IC_{50} = 80\,\mu M$, SPR $K_D = 51\,\mu M$), while the shorter aniline derivative **35** was inactive (FP $IC_{50} > 1000\,\mu M$). For further fine tuning of the optimal linker length, we evaluated the simple amides **36** and **37** with a methylene or ethylene spacer and an aniline substituent in the S2 pocket. In this case, the shorter methylene derivative **36** showed already a > 1000-fold improvement (FP $IC_{50} = 2.8\,\mu M$, PPIase $IC_{50} = 28\,\mu M$, SPR $K_D = 4.9\,\mu M$) compared to the millimolar potencies of **7** and **4**. In contrast, the longer ethylene analogue **37** was only weakly potent (FP $IC_{50} = 490\,\mu M$). This result corresponds well with the distance of 3.0 Å between the **7** carboxylic O-atom and the 3-fluorine atom in the overlay of the CypD·7·4 ternary complex with CypD·3 (Fig. 4).

Finally, we replaced the aniline of **36** with a tetrahydroquinoline substituent and the bicyclic fragment core **3** in the preferred stereochemistry (2*R*,3*R*,6*S*) yielding compounds **38**–**40** (Table 4).

The tetrahydroquinoline derivative **38** showed a 2-fold potency improvement (FP $IC_{50} = 1.35\,\mu M$, PPIase $IC_{50} = 0.6\,\mu M$, SPR $K_D = 1.6\,\mu M$) compared with **36**, but **38** has been tested as racemic mixture of the different bicyclic norbornane maleimides (exo and endo forms). The separated stereoisomers **39** (endo) and **40** (exo) indeed showed slight potency improvements regarding either the biochemical or SPR binding assays (**39**: FP $IC_{50} = 1.7\,\mu M$, SPR $K_D = 660\,nM$, **40**: FP $IC_{50} = 735\,nM$, SPR $K_D = 1.2\,\mu M$). We co-crystallized **40** in CypD (PDB-ID: 6R8W) and confirmed the fragment linking approach by clear identification of the bicyclic rings of **3** and **7** in the S2 and S1′ pockets respectively (Fig. 5). The binding orientation of the annulated tetrahydropyran ring of **40** in the S2 pocket corresponds with the fragment hit **3** or with the optimized urea **14**. In contrast, the electron density indicated two alternative conformations of the norbornane maleimide

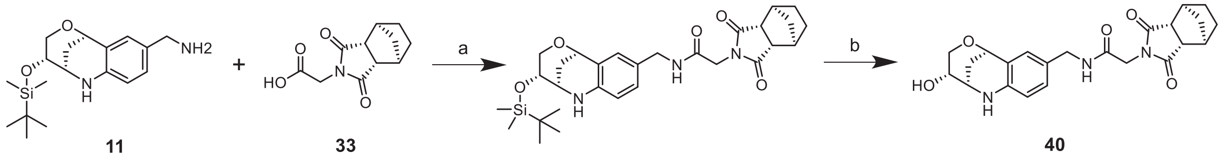

Scheme 3. Reagents and conditions: (a) EDCI, HOPO and DIPEA in DMF at 50 °C for 24 h; (b) TBAF in THF at RT for 20 h.

Table 4

CypD SAR of optimized amides derived from fragment linking of fragment hits **3** or **4** with fragment hit **7**.

#	Structure	Biochemical CypD FP assay		Biochemical PPIase assay IC_{50} (µM)[c]	SPR binding CypD	
		IC_{50} (µM)[a]	LE[b]		K_D (µM)[d]	LE[e]
34	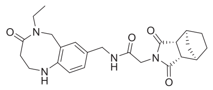	80	0.18	nt	ND	
35	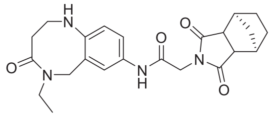	ND		nt	> 6000	
36	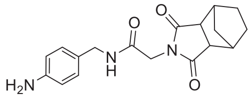	2.8	0.32	28	4.9	0.29
37	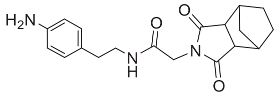	490	0.18	nt	> 200	
38	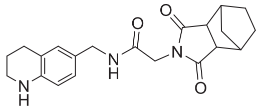	1.35	0.30	0.6	1.6	0.28
39	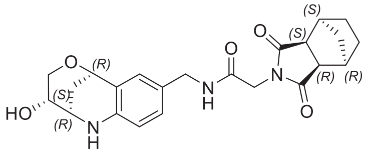	1.7	0.26	nt	0.660	0.26
40	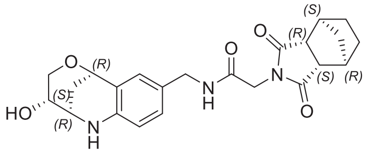	0.735	0.27	nt	1.2	0.25

[a,b]CypD biochemical FP and PPIase assays. [c,e]Ligand binding efficiencies (LE) based on biochemical FP IC_{50}s or SPR K_Ds. [d]CypD SPR binding assay. nt = not tested, ND = not detected.

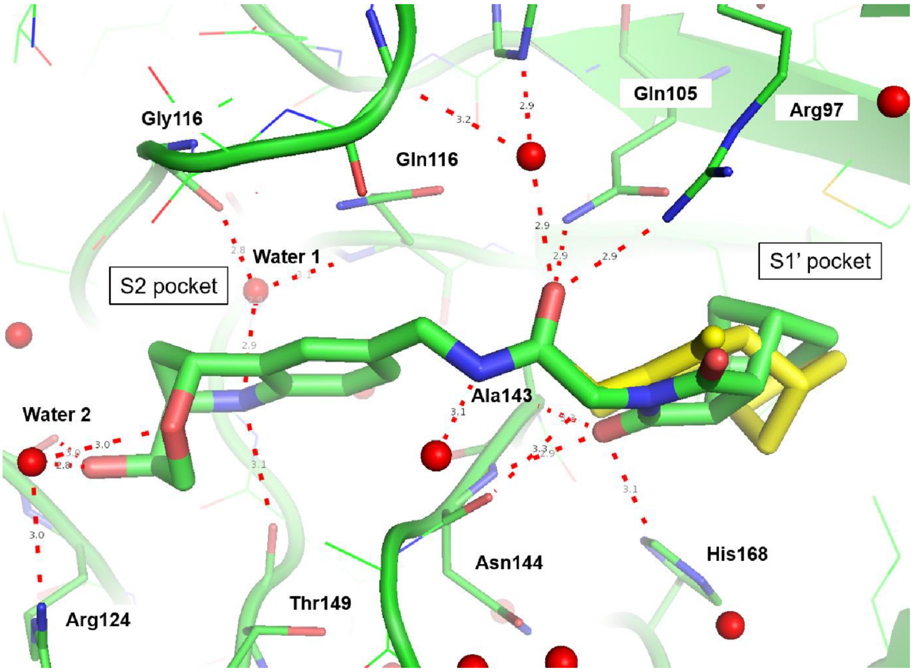
Gly116
Gln116
Gln105
Arg97
3.2
2.9
2.9
2.8
Water 1
2.9
2.9
S1' pocket
S2 pocket
2.9
Water 2
Ala143
3.0
3.1
3.1
3.3
2.9
3.1
3.0
Asn144
His168
Thr149
Arg124

Fig. 5. CypD X-ray structure in complex with the amide derivative **40** (PDB-ID: 6R8W) at 1.4 Å resolution, which was derived from fragment linking of **3** and **7**. The bicyclic ring of **3** is bound in the S2 pocket with specific H-bonds involving also water molecules 1 and 2. The bicyclic norbornane maleimide ring of fragment **7** binds in two alternative conformations (green and yellow) distinguished by 180° rotation in the S1′ pocket. In both orientations, the maleimide carbonyl O-atom is in H-bond contact to Asn144 and His168. The amide group connecting both fragments forms H-bonds to Arg97 (direct) and Gln116 and His (water mediated).

ring of **40** in the S1′ pocket. Both orientations are distinguished by 180° rotation of the maleimides ring (exo form) in the S1′ pocket resulting in nearly identical positions of the carbonyl O-atom in H-bond contact to Asn144 and His168. Consequently, the bicyclic norbornane ring adopts two alternative orientations in the S1′ proline pocket with vdW-interactions to Phe102, Phe155 and Met103. The amide linker of **40** forms H-bonds directly to Arg97 and Gln105 and water mediated H-bonds to Gly114 and His96.

In summary, our fragment-based approaches yielded three different series with either urea, oxalyl or amide linkers connecting millimolar fragments in the S1′ and S2 pockets. We successfully improved the in vitro CypD potencies in the biochemical FP assay and the biophysical SPR binding assays from millimolar towards the low and sub-micromolar range by > 1000-fold for some fragments. The initial SAR together with the protein crystal structures of our novel CypD inhibitors provide a suitable basis for further hit-to-lead optimization.

Accession codes

Coordinates and structure factors have been deposited to the protein data bank with codes 6R9S, 6R9U, 6RA1, 6R9X, 6R8L, 6R8O and 6R8W.

Declaration of Competing Interest

The authors declare that they have no known competing financial interests or personal relationships that could have appeared to influence the work reported in this paper.

Appendix A. Supplementary data

Supplementary data to this article can be found online at https://doi.org/10.1016/j.bmcl.2019.126717.

References

1. Viaud J, Subra G, Lin Y-L, et al. Structure-based design, synthesis, and biological evaluation of novel inhibitors of human cyclophilin A. *J Med Chem.* 2006;49(3):900–910. https://doi.org/10.1021/jm050716a.
2. Davis TL, Walker JR, Campagna-Slater V, et al. Structural and biochemical characterization of the human cyclophilin family of peptidyl-prolyl isomerases. *PLoS Biol.* 2010;8(7) https://doi.org/10.1371/journal.pbio.1000439.
3. Wang P, Heitman J. The cyclophilins. *Genome Biol.* 2005;6:7. https://doi.org/10.1186/gb-2005-6-7-226.
4. Liu Y, Jiang J, Richardson PL, Reddy RD, Johnson DD, Kati WM. A fluorescence polarization-based assay for peptidyl prolyl cis/trans isomerase cyclophilin A. *Anal Biochem.* 2006;356(1):100–107. https://doi.org/10.1016/j.ab.2006.04.040.
5. Handschumacher RE, Harding MW, Rice J, Drugge RJ, Speicher DW. Cyclophilin: a specific cytosolic binding protein for cyclosporin A. *Science (80-).* 1984;226(4674):544. https://doi.org/10.1126/science.6238408 LP – 547.
6. Huai Q, Kim H-Y, Liu Y, et al. Crystal structure of calcineurin-cyclophilin-cyclosporin shows common but distinct recognition of immunophilin-drug complexes. *Proc Natl Acad Sci USA.* 2002;99(19):12037–12042. https://doi.org/10.1073/pnas.192206699.
7. Giorgio V, Soriano ME, Basso E, et al. Cyclophilin D in mitochondrial pathophysiology. *Biochim Biophys Acta.* 2010;1797(6–7):1113–1118. https://doi.org/10.1016/j.bbabio.2009.12.006.
8. Forte M, Bernardi P. Genetic dissection of the permeability transition pore. *J Bioenergy Biomembr.* 2005;37(3):121–128. https://doi.org/10.1007/s10863-005-6565-9.
9. Elrod JW, Molkentin JD. Physiologic functions of cyclophilin D and the mitochondrial permeability transition pore. *Circ J.* 2013;77:1111–1122.
10. Panel M, Ruiz I, Brillet R, et al. Small-molecule inhibitors of cyclophilins block opening of the mitochondrial permeability transition pore and protect mice from hepatic ischemia–reperfusion injury. *Gastroenterology.* 2019. https://doi.org/10.1053/J.GASTRO.2019.07.026.
11. Dornan J, Taylor P, Walkinshaw MD. Structures of immunophilins and their ligand complexes. *Curr Top Med Chem.* 2003;3(12):1392–1409.
12. Ke H, Huai Q. Crystal structures of cyclophilin and its partners. *Front Biosci.* 2004;9:2285–2296.
13. Ahmed-Belkacem A, Colliandre L, Ahnou N, et al. Fragment-based discovery of a new family of non-peptidic small-molecule cyclophilin inhibitors with potent antiviral activities. *Nat Commun.* 2016;7. https://doi.org/10.1038/ncomms12777.
14. Hopkins S, Gallay P. Cyclophilin inhibitors: an emerging class of therapeutics for the treatment of chronic hepatitis C infection. *Viruses.* 2012;4(11):2558–2577. https://doi.org/10.3390/v4112558.
15. Ni S, Yuan Y, Huang J, et al. Discovering potent small molecule inhibitors of cyclophilin A using de novo drug design approach. *J Med Chem.* 2009;52(17):5295–5298. https://doi.org/10.1021/jm9008295.
16. Ahmed-Belkacem A, Colliandre L, Ahnou N, et al. Fragment-based discovery of a new family of non-peptidic small-molecule cyclophilin inhibitors with potent antiviral activities. *Nat Commun.* 2016;7:12777. https://doi.org/10.1038/ncomms12777.
17. Shore ER, Awais M, Kershaw NM, et al. Small molecule inhibitors of cyclophilin D to protect mitochondrial function as a potential treatment for acute pancreatitis. *J Med Chem.* 2016;59(6):2596–2611. https://doi.org/10.1021/acs.jmedchem.5b01801.
18. Hopkins AL, Keseru GM, Leeson PD, Rees DC, Reynolds CH. The role of ligand efficiency metrics in drug discovery. *Nat Rev Drug Discov.* 2014;13(2):105–121. https://doi.org/10.1038/nrd4163.
19. Siegal G, Ab E, Schultz J. Integration of fragment screening and library design. *Drug Discov Today.* 2007;12(23–24):1032–1039. https://doi.org/10.1016/j.drudis.2007.08.005.
20. Schlatter D, Thoma R, Küng E, et al. Crystal engineering yields crystals of cyclophilin D diffracting to 1.7 Å resolution. *Acta Crystallogr Sect D Biol Crystallogr.* 2005;61(5):513–519. https://doi.org/10.1107/S0907444905003070.
21. Jorand-Lebrun C, Johnson TL, Graedler U, et al. Preparation of urea and amide compounds for the inhibition of cyclophilins. PCT Int Appl 2017;(WO2017173048A1):95pp.
22. Kuhn B, Fuchs JE, Reutlinger M, Stahl M, Taylor NR. Rationalizing tight ligand binding through cooperative interaction networks. *J Chem Inf Model.* 2011;51(12):3180–3198. https://doi.org/10.1021/ci200319e.
23. Jorand-Lebrun C, Johnson TL, Graedler U, et al. Preparation of oxalyl compounds for the inhibition of cyclophilins. PCT Int Appl 2017;(WO2017173049A1):61pp.
24. Jorand-Lebrun C, Johnson TL, Graedler U, Jiang X, Kulkarni S. Preparation of dioxohexahydroisoindolyl compounds for the inhibition of cyclophilins. PCT Int Appl 2017;(WO2017173052A1):56pp.